C09/1*

Fuel Assembly Loads during a Hypothetical Blowdown Event in a PWR

J. STABEL, B. BOSANYI, J. D. KIM
Siemens Aktiengesellschaft, Erlangen, FRG

ABSTRACT

As a consequence of a hypothetical sudden break of the main coolant pipe of a PWR, RPV-internals and fuel assemblies (FA's) are undergoing horizontal and vertical motions.

FA's may impact against each other, against core shroud or against lower core support. The corresponding impact loads must be absorbed by the FA spacer grids and guide thimbles. In this paper FA-loads are calculated with and without consideration of Fluid-Structure-Interaction (FSI) effects for assumed different break sizes of the main coolant pipe. The analysis has been performed for a hypothetical cold leg break of a typical SIEMENS-4 loop plant.

For this purpose the codes DAPSY/DAISY (GRS, Germany) were coupled with the structural code KWUSTOSS (SIEMENS).

It is shown that the FA loads obtained in calculations with consideration of FSI effects are by a factor of 2-4 lower than those obtained in the corresponding calculations without consideration of FSI.

1 INTRODUCTION

By the postulated sudden break of a main coolant pipe, pressure waves are generated which impose forces on RPV, RPV-internals and core components.

The resulting motion is strongly influenced by FSI effects taking place in the annular gap between RPV and core barrel: Pressure differences constitute forces acting on the structure; on the other hand the fluid pressure is strongly influenced by the structural motion.

We performed calculations with and without consideration of FSI effects. In the calculations without consideration of FSI effects in the downcomer the structural motion of RPV and core barrel is not transferred to the fluid equations.

The total model comprehends a hydraulic model of the total primary circuit, further a hydraulic and a structural model of RPV, RPV-internals and core components. The hydraulic and structural model of RPV and internals is based on /1/. In addition to

SMiRT 11 Transactions Vol. C (August 1991) Tokyo, Japan,

this work the model of the RPV internals was considerably improved.
Further we introduced detailed models of
- the RPV (as rigid beam structure) with RPV-support
- and the fuel assemblies
into the global model.

The equations of motion were partially vectorized in order to minimize the computational time. For the same purpose of computational optimization, four different subcycles were used in the integration scheme (for the fluid equations, for the shell equations of RPV-internals, for the horizontal motion of the fuel assemblies, for the vertical motion of the fuel assemblies).

This model allows to analyze the effect of various break sizes on the structural loads. In this report the emphasis is laid on the modelling of the fuel assemblies and discussion of corresponding results.

2 HYDRAULIC MODEL

The hydraulic modelling is done with the fluid code DAPSY /1/.

The base of DAPSY consists of one-dimensional 'fluid-pipes'. Two- and three-dimensional geometries can be modelled with the aid of a network technique.

This is the case for the fluid annular gap between RPV and core barrel.

DAPSY models a homogeneous two-phase fluid flow by the consideration of 4 equations:
- two equations for the conservation of mass (for the two phases)
- one equation for the conservation of momentum
- one equation for the conservation of energy.

A delayed attainment of thermodynamic equilibrium is considered.

The equations are numerically integrated in an explicit scheme by the method of characteristics.

The initial values for the thermodynamic state variables are determined by an explicit or implicit algorithm, as one chooses.

Different boundary conditions such as
- various types of break opening functions over time (subcritical and critical flow conditions)
- valves
- pumps
- branchings and links

can be adequately considered.

Spatial and temporary changes of the size of the annular gap between RPV and core barrel due to the structural motion are calculated and introduced in the fluid equations (FSI effect) for all calculations 'with FSI'.

The hydraulic model of one loop of the primary circuit is shown in fig. 1. In this case a double-ended break (2A-break) is simulated with the aid of the pipes 385, 396 and the valve between 395 and 394. Within 15 ms the pipes 385 and 396 will completely open, within the same time the valve will close. The

other break situations considered later on parametrically, namely 0.5A break and 0.1A break, are modelled by similar techniques.

Fig. 2 shows the fluid model for RPV-internals and core components. Fig. 3 shows the development of the fluid model for the annular region between RPV and core barrel.

3 RPV AND RPV-INTERNALS MODEL

The RPV-internals (core barrel, upper and lower core support, grid plate and core shroud) are modelled by appropriate structural elements.

Fig. 4 shows the development of the core barrel /1/.
The structural equations of the RPV-internals as well as the FSI in the downcomer are formulated by the code DAISY.

The RPV is a very stiff structure and it is sufficient to model it by a rigid beam. The characteristics of the RPV support are fully considered.

A possible sliding of the core barrel flange has also been adequately modelled.

In the analysis not the total model but only a condensed model of the RPV-internals is used.

The condensed model has the following degrees of freedom (d.o.f.):

- 256 radial d.o.f. for defining FSI between structural parts (core barrel and RPV) and the downcomer fluid region
- 16 radial, 16 tangential and 16 axial d.o.f. for defining core barrel sliding
- 4 tangential d.o.f. for defining the coupling of the grid plate to the core barrel.

The corresponding structural matrices (mass matrix, damping matrix, stiffness matrix) have the dimensions 308x308 and are fully occupied.

The structural equations of motion are integrated by central differences, hereby the corresponding matrix-vector operations are fully vectorized.

Further, the core is coupled via grid plate, core shroud and lower core support plate directly to the core barrel. Core and core barrel may interact by impact forces imposed by the fuel assemblies on the core shroud. The pressure waves generated by a LOCA event will also accelerate the core in vertical direction. Hereby the sliding behaviour of the core barrel flange is influenced.

All of these phenomena:

- coupling of the horizontal motions of core and core barrel
- coupling of the vertical motion of core and the horizontal motion of core barrel via core barrel flange

are fully considered and modelled in detail.

4 FUEL ASSEMBLY (FA) MODEL

We consider the core of a 4-loop plant with 193 FA's (fig. 5). As a consequence of the blowdown event the FA's will vibrate in the 2 horizontal directions and in the vertical direction.

The FA's are arranged in rows of different length (7-, 11-, 13- and 15-FA-rows). Between neighbouring FA's we have a certain gap. As soon as this gap is closed, the FA's will impact against each other or against the core shroud.

The motion of a total FA-row depends on the sum of the gaps in this row, i. e. on the number of FA's in the specific row considered.

For the modelling of the horizontal vibration of the core we assume:

- the vibration in the two principal directions is independent from each other
- the motion of two different rows of equal length in any of the two principal directions is the same.

Therefore the motion in each of the two principal horizontal directions can be represented by 4 'equivalent' FA-row-models of different length.

This means, for example, that the seven 15-FA-rows in x-direction (see fig. 5) have been gathered up to one 'equivalent' 15-FA-row in x-direction.

Fig. 6 shows for example a 7-FA-row-model.

Hereby the total horizontal motion of the core is modelled by $2x(7+11+13+15) = 92$ FA's.

Each FA has 25 nodes, each node has 4 degrees of freedom (1 translation, 1 rotation and the corresponding velocities).

The row models are excited via grid plate, core shroud and lower core support plate. On the other hand impact forces imposed by the FA's are acting on the core barrel structure.

The mechanics of the FA-row-models will be explained later on in detail.

In addition to the horizontal motion of the core we must also consider a vertical motion of the core.

The FA's are vertically accelerated by pressure differences which are evaluated in the hydraulic model of the core (see fig. 2).

For reasons of consistency between the vertical structural model and the hydraulic model of the core, we assume that the vertical motion of the core is the same for all FA's (see fig. 2, fig. 7).

The vertical structural model of the core is a highly nonlinear mechanical model. The contact between the bottom end pieces and the lower core support resp. between the top end pieces and the grid plate (holddown device) are appropriately taken into consideration. Further the guide thimble and fuel rod stiffnesses as well as the sliding contact between the spacer grids (fixed to the guide thimbles) and the fuel rods are modelled in detail.

The corresponding equations of motion are integrated by an explicit 4 step Runge-Kutta algorithm.

Hereby the total modelling of the horizontal and vertical motion of the core is fully described.

Now we turn once again to fig. 6 and have a look on the detailed horizontal FA-model /2/.

The FA's are connected by horizontally acting springs to the lower core support 1 and the grid plate 2 (centering pins!). Further they are directly coupled by nonlinear contact elements to neighbouring nodes of the RPV internals model (nodes 3-10 and 11-18).

The FA's are modelled by lumped masses which are connected by equivalent beam elements.

Different linear and nonlinear damping mechanisms are used.

The interaction between neighbouring FA's or between FA's and RPV-internals is modelled by a series connection of a linear spring and a nonlinear spring with gap. Hereby one- and two-sided (through-grid) impacts can be appropriately modelled.

The nonlinear impact springs, e.g. coupling 143-151, represent the spacer grid (SG) through grid stiffness.

Possible elasto-plastic deformations of the SG can also be taken into account.

All of the relevant model data are validated by experimental results. The equations of motion are explicitly integrated by a 4 step Runge-Kutta algorithm, optionally in connection with a mixed explicit/implicit strategy for the integration of the impact phenomena.

5 RESULTS

Three break situations namely a 2A-, a 0.5A- and a 0.1A-break with a linear break size opening within 15 ms were parametrically investigated. We performed, as explained above, calculations with and without consideration of FSI effects. This constitutes one parameter of the analysis. The other parameter considered refers to the elasto-plastic deformation behaviour of the FA-SG's.

On the one hand we perform a realistic 'elasto-plastic analysis' with an experimentally verified finite limit for the beginning of elasto-plastic SG-deformation. Here the elasto-plastic SG-deformation behaviour is fully considered.

On the other hand we perform a hypothetical 'elastic analysis' with an assumed infinitely high limit for the beginning of elasto-plastic deformation. This analysis is mainly done for the purpose of comparison between calculations with and without consideration of FSI effects.

As for the results of the different analyses, the emphasis is laid on comparison of the SG-impact loads. The motion of the core barrel determines the FA-loads.

Fig. 8, 9 show the radial core barrel motion at the entry of the break loop into the RPV.

We identify that

- the initial gradient of the core barrel motion is much steeper for the analyses 'without FSI' (⇒ higher loads)
- the core barrel motions for 2A- and 0.5A-break size are similar

- the core barrel motions are limited in size by impacting of the core barrel flange against the RPV.

It should be noted that maximum loads occur at the periphery of the core.

Table 1 shows for the 3 break situations the maximum impact loads on the FA's for an 'elastic analysis' with and without FSI.

We identify that the SG-Loads for the realistic calculations 'with FSI' are lower by a factor between 2 - 4, depending on the break size, than the corresponding loads from calculations 'without FSI'.

It turns out that the elasto-plastic analyses differ from the above calculations only in the cases 2A-break with and without FSI and 0.5A-break without FSI.

Table 2 shows the maximum elasto-plastic SG-deformations.

It is remarkable that the maximum loads for the calculations 'without FSI' are occurring at the very beginning of the blowdown when the core shroud is impacting for the first time against the FA's.

At this moment the calculation predicts a total of 105 SG's in the core to be deformed plastically (2A-break without FSI).

Fig. 10, 11 show for the cases 2A- and 0.5A-break the deformed spacers for the 7-FA-model in x-direction.

For the calculations 2A-break 'with FSI' the maximum loads of the SG's will occur in a later phase of the blowdown, when the core barrel is swinging back and correspondingly at the FA's on the other side of the core.

Plastic deformations will occur in this case only in the 7-FA-row; the calculated deformation is much lower than 1 mm. Only 2 SG's in the core are deformed plastically one in each 7-FA-row (see fig. 10).

Fig. 12 shows for the case 2A-break with FSI the resulting impact loads and displacements at the periphery of the 7-FA-model at the 7th SG level in x-direction.

From figure 12a we identify that at time T ≈ 17 ms the core shroud is impacting against one peripheral FA.

From figure 12b we identify that at time T ≈ 55 ms the core shroud is swinging back against the other side of the 7-FA-row model. Maximum loads occur at this point of time, the impacting SG is slightly deformed plastically.

Neither the coolability of the core nor the free path of control rods is impaired by these SG-deformations.

6 CONCLUSIONS

It was shown that computer codes which don't consider FSI-effects in the downcomer will over-estimate the FA-loads in the SG-levels by a factor of 2-4. Due to the nonlinearity of the total mechanical model, the exact value of this factor depends on the break size as well as on the structural and hydraulic properties of the whole system.

7 REFERENCES

/1/ D. Müller-Ecker, S.E. Meier, P. Gruner
Analysis of a PWR-Primary-System Under Blowdown Loading with the Fluid-Structure Interaction Code DAISY
SMIRT 1985, F1 1/3

/2/ J.D. Kim, U. Borsdorf, H.P. Fuchs, J. Stabel
Influence of Energy Dissipation on PWR Fuel Assembly Behaviour During Severe Seismic Excitation
SMIRT 1989

8 ACKNOWLEDGEMENTS

We thank the GRS Köln, in particular Mr. Dr. Meyer and Mr. Bartalsky, for many substantial discussions on DAPSY/DAISY. Further we thank our colleagues from the SIEMENS-RPV-internals and -FA departments for the contribution of various input data.

Table 1: Maximum SG-impact loads for 'elastic' analyses

break size	max. SG-loads with FSI (kN)	max. SG-load without FSI (kN)
0.1A	4	15
0.5A	16	41
2A	25	62

Table 2: Maximum plastic SG-deformations for 'elasto-plastic' analyses

break size	max. plastic SG-deformations with FSI (mm)	max. plastic deformations without FSI (mm)
0.1A	-	-
0.5A	-	2.0
2A	<< 1	3.1

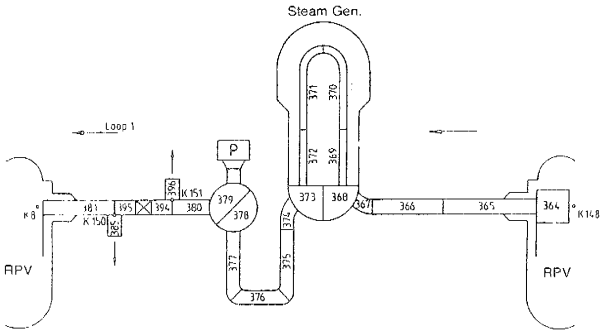

Fig. 1: Fluid model of Loop 1 (Loop of hypothetical 2A-break) /1/

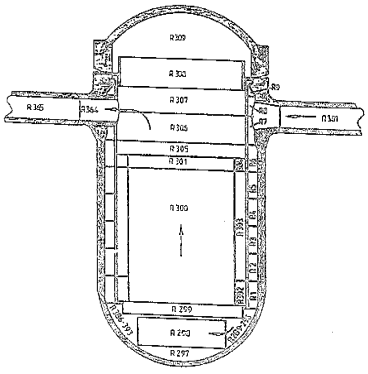

Fig. 2: Fluid Model for RPV Internals and core /1/

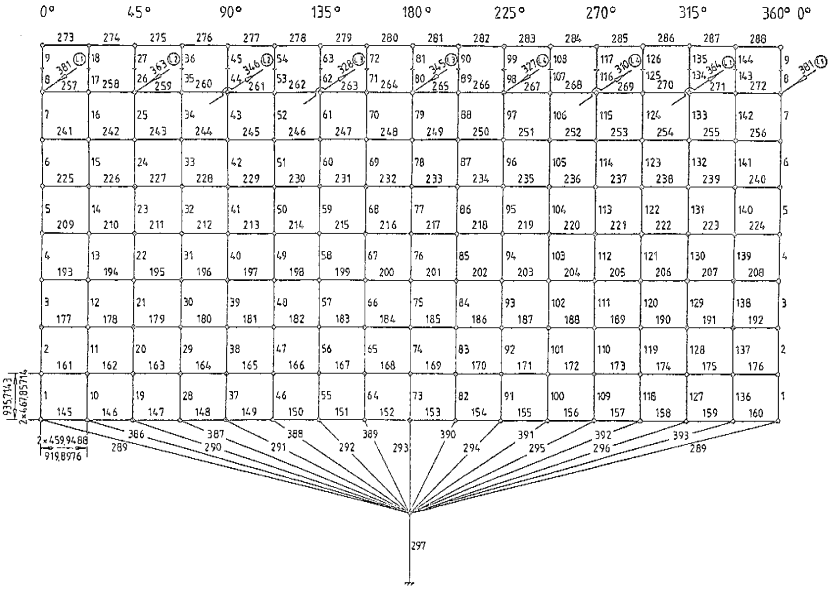

Fig. 3: Fluid Model for annular region between RPV and core barrel (development) /1/

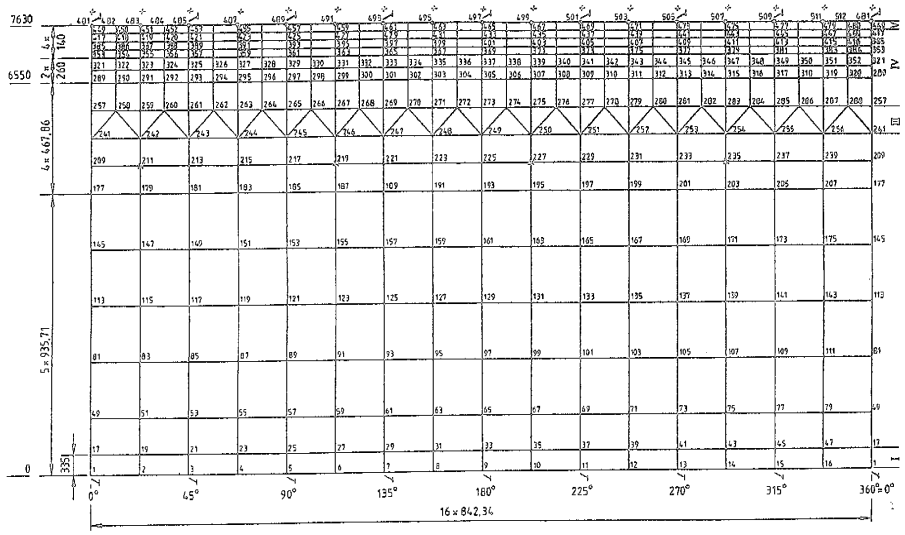

Fig. 4: Structural Model of Core Barrel (development) /1/

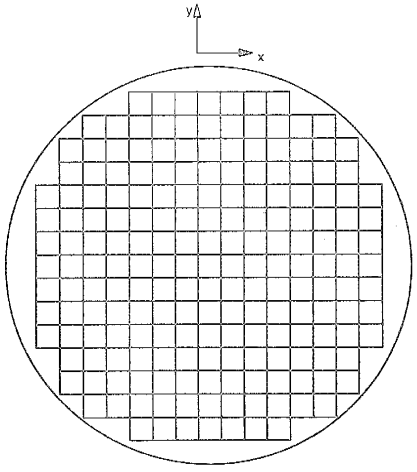

Fig. 5: Core scheme of a 4 loop PWR

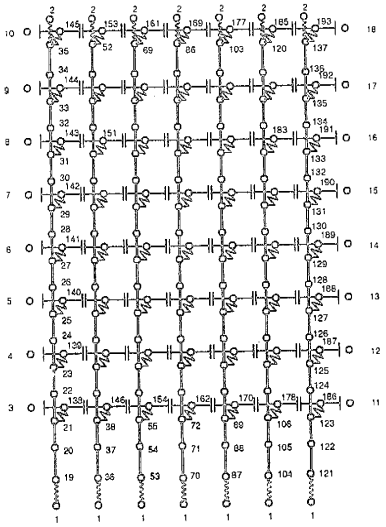

Fig. 6: 7–FA–row–Model

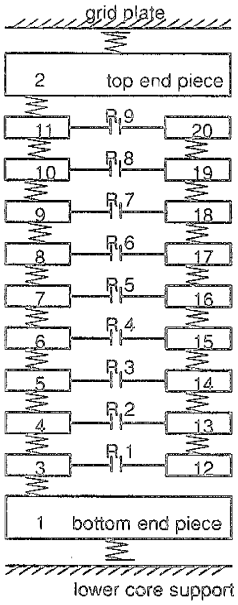

Fig. 7: Vertical Structural Model of the Core

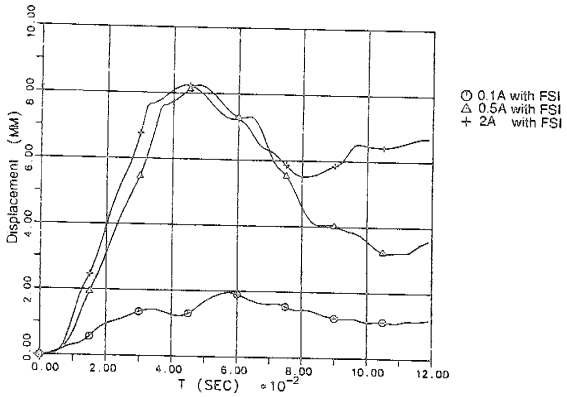

Fig. 8: Displacements of the Core barrel at entry of the break loop in the RPV (with 'FSI')

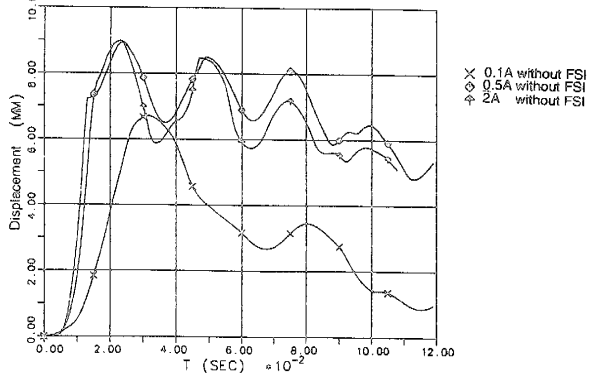

Fig. 9: Displacements of the Core barrel at entry of the break loop in the RPV (without 'FSI')

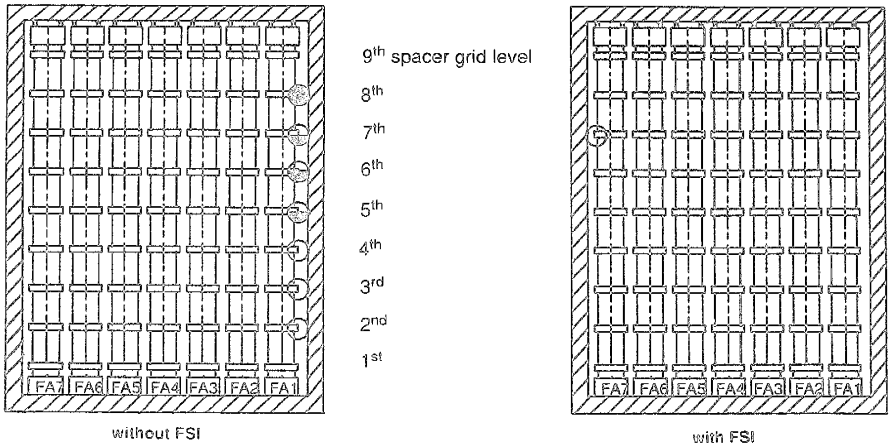

Fig. 10: Elasto–Plastic SG–Deformations for 2A–break

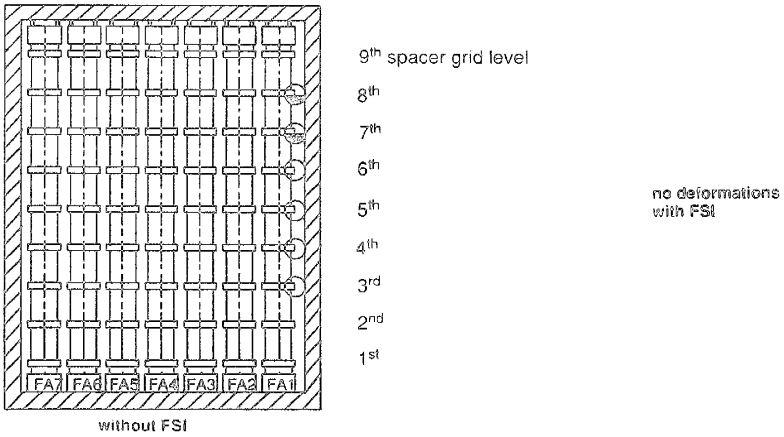

Fig. 11: Elasto–Plastic SG–Deformations for 0.5A–break

legend: : $x_b > 3$ mm

: 1mm < x_b < 3 mm

: $x_b < 1$ mm

x_b = plastic SG–deformation

Node–numbering: see fig. 6

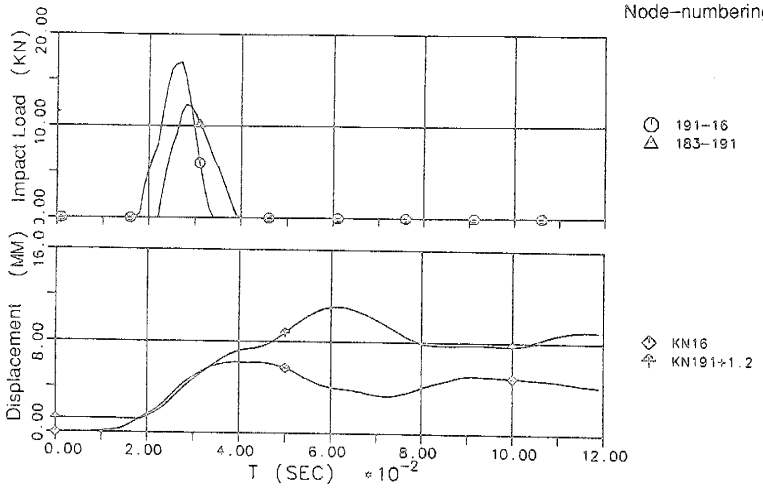

Fig. 12a: 2A–break with FSI; FA in x–direction (7th SG level)

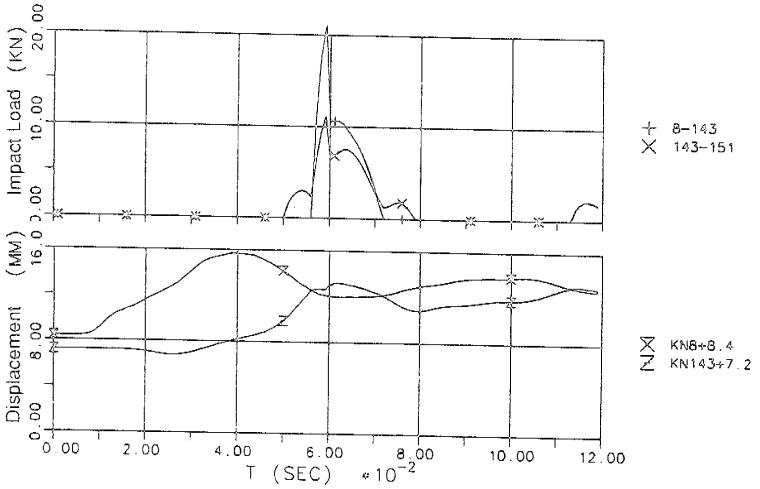

Fig. 12b: 2A–break with FSI; FA in x–direction (7th SG level)